NeuroImage 82 (2013) 595–604

Contents lists available at ScienceDirect

NeuroImage

journal homepage: www.elsevier.com/locate/ynimg

Functional brain network organisation of children between 2 and 5 years derived from reconstructed activity of cortical sources of high-density EEG recordings

Joe Bathelt [a,*], Helen O'Reilly [a,b], Jonathan D. Clayden [a], J. Helen Cross [a], Michelle de Haan [a]

[a] University College London Institute of Child Health, UK
[b] University of Cambridge Autism Research Centre, UK

ARTICLE INFO

Article history:
Accepted 2 June 2013
Available online 12 June 2013

Keywords:
EEG
Electroencephalogram
Development
Connectivity
Network
Source analysis
Paediatric
Minimum-norm estimation

ABSTRACT

There is increasing interest in applying connectivity analysis to brain measures (Rubinov and Sporns, 2010), but most studies have relied on fMRI, which substantially limits the participant groups and numbers that can be studied. High-density EEG recordings offer a comparatively inexpensive easy-to-use alternative, but require channel-level connectivity analysis which currently lacks a common analytic framework and is very limited in spatial resolution. To address this problem, we have developed a new technique for studies of network development that overcomes the spatial constraint and obtains functional networks of cortical areas by using EEG source reconstruction with age-matched average MRI templates (He et al., 1999). In contrast to previously reported channel-level analysis, this approach provides information about the cortical areas most likely to be involved in the network as well as their functional relationship (Babiloni et al., 2005; De Vico Fallani et al., 2007).
In this study, we applied source reconstruction with age-matched templates to task-free high-density EEG recordings in typically-developing children between 2 and 6 years of age (O'Reilly, 2012). Graph theory was then applied to the association strengths of 68 cortical regions of interest based on the Desikan–Killiany atlas. We found linear increases of mean node degree, mean clustering coefficient and maximum betweenness centrality between 2 years and 6 years of age. Characteristic path length was negatively correlated with age. The correlation of the network measures with age indicates network development towards more closely integrated networks similar to reports from other imaging modalities (Fair et al., 2008; Power et al., 2010). We also applied eigenvalue decomposition to obtain functional modules (Clayden et al., 2013). Connection strength within these modules did not change with age, and the modules resembled hub networks previously described for MRI (Hagmann et al., 2010; Power et al., 2010). The high temporal resolution of EEG additionally allowed us to distinguish between frequency bands potentially reflecting dynamic coupling between different neural oscillators. Generally, network parameters were similar for networks based on different frequency bands, but frequency band did emerge as a significant factor for clustering coefficient and characteristic path length. In conclusion, the current analysis shows that source reconstruction of high-density EEG recordings with appropriate head models offers a valuable tool for estimating network parameters in studies of brain development. The findings replicate the pattern of closer functional integration over development described for other imaging modalities (Fair et al., 2008; Power et al., 2010).

Introduction

Recent advances in brain imaging and analysis highlight the importance of interplay between brain regions. Rather than investigating the role of individual brain regions for specific functions, brain connectivity analysis describes the dynamic engagement of multiple brain regions (brain 'networks'). The specific regions identified using various imaging methods differ, probably because the physiological processes underlying different imaging modalities are not the same (Darvas et al., 2004; He et al., 2011). However, graph theory provides a common mathematical framework to compare the network architecture (Rubinov and Sporns, 2010), even when the anatomical regions are not identical. The network architecture was shown to be similar across different scales (Van den Heuvel et al., 2008; Watts and Strogatz, 1998). In this article, we describe a method that allows characterisation of functional cortical networks from high-density EEG recordings in children from 2 years of age.

Functional connectivity measures of the brain can in principle be derived from all functional imaging data such as fMRI, EEG, MEG, and near-infrared spectroscopy (NIRS), but the current literature is

* Corresponding author at: Developmental Cognitive Neuroscience Unit, UCL Institute of Child Health, 30 Guilford Street, WC1N 1EH London, UK.
E-mail address: johannes.bathelt.10@ucl.ac.uk (J. Bathelt).

1053-8119/$ – see front matter.
http://dx.doi.org/10.1016/j.neuroimage.2013.06.003

mostly based on findings from fMRI. A consistent finding in the functional connectivity MRI (fcMRI) literature is the presence of an interconnected network comprising the medial prefrontal cortex, the posterior cingulate, the inferior parietal lobe, the lateral temporal cortex and the hippocampal formation during the resting state (Cherkassky et al., 2006; Fox and Raichle, 2007; Shulman et al., 1997). This network was named the default mode network (DMN). It is thought to be one of the three major networks that are reciprocally regulated (Menon, 2011). The great advantage of the DMN is that it can be investigated even if the participant is not engaged in a task, which is particularly useful in groups with limited cooperative ability like children or developmentally delayed patients. Further, patients and controls can be compared without the assumption that the groups use similar strategies for solving a task. Due to the interplay between functional networks, the characterisation of one network provides an impression of overall functional integrity. Assessment of the resting-state functional connectivity has been widely used to characterise brain development and pathophysiology.

The development of resting-state functional connectivity has been investigated with various techniques. Homae et al. report the development of functional networks in neonates and infants of up to 6 months of age using NIRS (Homae et al., 2010). They collected NIRS data while the children were asleep and calculated correlations between the time series of the channels. They reported an increase in correlation between channels in posterior regions and a decrease in frontal regions. Similarly, Thatcher and colleagues used EEG coherence to investigate the development of cortical functional connectivity in a large sample of age groups between 2 months and 16 years (Thatcher et al., 2008). They report stronger coherences with age, increased anterior–posterior connections and a decrease in overall coherence between electrodes with longer distances (Barry et al., 2004). This is in line with functional connectivity analysis of fMRI data reported by Fair and colleagues that compared the rs-fcMRI architecture of school-age children with adults. The authors found that 7 to 9 year old children display little functional connectivity between the mPFC and posterior cingulate and parietal regions compared to adults. These areas appear highly integrated in adults. In contrast, there is a comparable degree of interhemispheric connections between homotopic regions in both children and adults, e.g. parahippocampal and superior frontal regions. A statistical comparison of connectivity between children and adults shows that the most pronounced differences are generally found in anterior-to-posterior connections. The decrease in correlation between regions is likely to reflect segregation of sub-networks that subserve different functions and integration of areas that mediate the same function (Thatcher et al., 2008). Increased connectivity between regions that are spatially segregated is likely to reflect functional integration (Uhlhaas et al., 2009; Uhlhaas et al., 2010).

The heavy reliance on fMRI to study development of functional connectivity may be due to limitations in the alternative tools. NIRS has been applied to study development of functional networks in sleeping neonates and infants of up to 6 months of age (Homae et al., 2010). However, as NIRS relies on light penetrating through the skull it is limited to infants and not suitable to study the full span of development. MEG offers excellent time and spatial resolution. However, magnetometers are expensive and not widely available. Further, MEG is less sensitive to deep or radially oriented sources (Michel and Murray, 2011). Additionally, the head coils used in magnetometers have a fixed size optimised for adults limiting their use for developmental studies. While these factors may have biased researchers towards fMRI, it also has limitations as very young children often require general anaesthesia or sedation for MRI. Further, MRI is costly and requires dedicated staff. Further, fMRI and NIRS measure differences in properties of oxygenated and de-oxygenated haemoglobin. The relationship between the BOLD signal and neural activity is indirect (Logothetis, 2008; Palmer, 2010) and BOLD response is temporally limited to slow fluctuation.

In contrast to fMRI, MEG, and NIRS, high-density EEG recordings provide several advantages for use in young children as they are not as sensitive to movement artefact, can be obtained across a wide range of age and ability levels, and are generally less costly. EEG directly measures brain electrical activity on the surface of the skull. Most EEG activity is generated by membrane potential fluctuations of cortical pyramidal cells perpendicular to the skull (Buzsàki et al., 2012). The excellent temporal resolution of the EEG, also allows the different physiological processes thought to manifest in different frequency bands to be distinguished. Oscillations in the lower part of the EEG power spectrum are associated with changes in membrane potential (Miller, 2007), whereas fast oscillations (>25 Hz) are linked to local field potentials (Buzsàki et al., 2012; Whittingstall and Logothetis, 2009). Generally, it is reported that the connectivity maps derived from different frequency bands are very similar (Barry et al., 2004; Murias et al., 2007) reflecting similar architectural constraints at different physiological levels (Bullmore and Sporns, 2009; Van den Heuvel et al., 2008). In summary, high-density recordings of EEG are inexpensive, easy to obtain even in young children and offer excellent temporal resolution. A great advantage of functional connectivity based on reconstructed EEG sources is the ease of application in populations that are not able to undergo MR scanning.

In spite of these advantages, one reason why researchers may not have embraced the use of EEG to study functional cortical networks is because of their limited spatial resolution. In order to overcome this barrier and obtain functional networks of cortical areas, we used EEG source reconstruction with age-matched average MRI templates (He et al., 1999). In contrast to previously reported channel-level analyses, this approach provides information about the cortical areas that are most likely to be involved as well as their functional relationship (Babiloni et al., 2005; De Vico Fallani et al., 2007) (Table 2). Further, the independence of nodes in the network is less confounded than in channel-level analysis, which does not take volume conduction effects into account.

Irrespective of the imaging modality, network analysis results in a measure of association strength between areas of interest. The properties of the resulting networks can be characterised through the mathematical framework of graph theory (Bullmore and Sporns, 2009; De Vico Fallani et al., 2007; Sporns, 2002). We applied commonly used graph measures such as node degree, average path length and clustering coefficient (Bullmore and Sporns, 2009; Chu-Shore et al., 2011). These measures allowed qualitative comparison of the characteristics of functional networks derived from reconstructed EEG sources to the organisation of networks derived in other studies using other imaging modalities like fMRI, NIRS etc. Furthermore, graph theory has been used to quantify the efficiency of a variety of networks. Most networks display a characteristic network organisation that is optimised for a) maximal processing speed b) minimal wiring cost and c) resilience (Watts and Strogatz, 1998). These networks all display a high level of local connectivity with some long-range connections. This has been described as a small-world architecture. Network analysis of structural and functional MRI data reveals that the human brain shares this organisation with other biological and non-biological networks, like neurons in *Caenorhabditis elegans* and traffic on the world-wide web (Bullmore and Sporns, 2012; Watts and Strogatz, 1998; Yu et al., 2008). We obtained measures so that the plausibility of functional networks derived from reconstructed EEG sources can be assessed qualitatively by comparing them to the characteristics of networks described in previously published reports that were derived from these other imaging modalities.

Materials and methods

Participant sample

The data were collected as a control sample for a study of children with epilepsy (O'Reilly, 2012). The control sample consisted of 47

children (22 female) between the ages of 1.5 and 6 years. Children older than 3 years were administered the British Picture Vocabulary Scale (Dunn and Whetton, 1982). For children less than 3 years, the parents were asked to complete the MacArthur communication development inventory — words and sentences (Essex et al., 2002). All children had to score above the 16th percentile (−1 standard deviation or above) on the BPVS or the vocabulary production subtest of the MacArthur to be included.

Procedure

EEG was recorded while children watched a video clip of calming scenes for 2 min in a dimly lit room. The video helped the children to sit still for the time required and to minimise their eye movements. The video was provided by the Brain and Cognitive Development Centre, Birkbeck College London.

The children were video-recorded to assess the degree of attentiveness. Children that were not engaged in watching the video (sleepy, upset) or otherwise engaged (talking to their caregiver, playing with object and not watching the screen) were excluded from the analysis (n = 8). Children who were younger than 24 months were excluded from the analysis, because the fontanelles are not likely to be fully closed (n = 4). The fontanelles in the skull violate the assumption of closed spheres of the boundary elements models that were used for source reconstruction in this study (Hämäläinen and Ilmoniemi, 1994; He et al., 1999). The total sample of EEG recordings that entered the analysis consisted of 36 recordings.

EEG recording

The EEG was recorded using EGI Geodesic Dense Array Sensor Nets with 128 electrodes against a vertex reference with the EGI Net Amp 200 Amplifier with NetStation 4.2 software at a sampling frequency of 250 Hz and a hardware bandpass filter of 1–100 Hz (Electrical Geodesics, Inc., Eugene, Oregon). The head circumference of each participant was measured prior to recording and a sensor net appropriate for the head size was used. The sensor net was aligned to nasion, inion and left and right pre-auricular points. The attachment and function of sensors were tested prior to recording with impedance measures.

EEG preprocessing

The EEG recordings were segmented into 1 s epochs. The segmented recordings were visually inspected. Segments that contained movement artefacts were excluded from the analysis. EEG channels that contained a high-level of noise or flat lines were rejected. The EEG was filtered using a high-pass, 4th order Butterworth filter with a cut-off frequency of 1 Hz and a similar high-pass filter with a cut-off at 40 Hz. The filtered and artefact-corrected EEG was re-referenced to average reference. Channels with a peak-to-peak amplitude larger than 100 μV were excluded for individual segments. Recordings that had more than 20% of trials or more than 20 channels rejected were excluded from further analysis (n = 2).

Source reconstruction

Boundary-element models (BEM) were calculated from average MRIs taken from the Neurodevelopmental MRI database[1] using FreeSurfer software v5.1.0 (Dale et al., 1999; Fischl et al., 1999) and MNE suite v2.7.0 (Hämäläinen and Ilmoniemi, 1994) under Mac OS 10.7.4 (Apple Inc., CA). BEMs consisted of three shells comprising the cortex, skull and skin. Each layer was calculated from the average MRI with FreeSurfer surface reconstructions. A cortical surface tessellation with 9750 vertices was used. BEMs were calculated for average MRIs for children from 2 years to 6 years in 0.5 year intervals (Evans, 2006; Sanchez et al., 2012).

The cortical reconstructions were parcellated into regions of interest (ROI) using FreeSurfer[2] (Fischl et al., 2004) according to the Desikan–Killiany atlas. This resulted in a total of 68 cortical regions of interest with 34 identical regions in each hemisphere.

The inverse solution was calculated for individual EEG segments using minimum-norm estimates (L2-normed, depth-weighted MNE). We used the inverse solution implemented in Brainstorm v3.1[3] (Sylvain et al., 2011) for source reconstruction. We used L2-normed, weighted MNE based on previous reports that this source inversion algorithm is well-suited for large-scale functional connectivity networks (He et al., 2011).

The connectivity was analysed in three frequency bands. The recordings were low-pass and high-pass filtered using digital 6th order Butterworth filters to isolate the frequency bands of interest. Frequencies between 1 and 12, 12 and 25 and 25–40 Hz were analysed. These correspond to the canonical delta/theta/alpha, beta and low gamma frequency bands. Neural oscillations measured by EEG display changes over development [1, 2]. Particularly slow wave oscillations in the theta and alpha range change dramatically in childhood (Marshall et al., 2002; Stroganova and Orekhova, 2007). One of the most dominant oscillations is the alpha rhythm. Young children show a dominant frequency in the EEG power spectrum between 5 and 8 Hz, whereas adults show a dominant frequency between 8 and 12 Hz. Because the current study investigates the development over a wide age range, we chose a wide frequency range in the lower power spectrum that would incorporate the dominant frequency in all age groups. We calculated source activity in each frequency band and derived the time series of cortical ROIs using Brainstorm algorithms v3.1 (Sylvain et al., 2011).

Connectivity

The time series of cortical ROIs derived from the EEG segments were correlated in pairwise correlations (Fig. 1). The average connectivity for a 1 s segment was calculated for individual participants and thresholded with the average connectivity (Hipp et al., 2012). A relative threshold was chosen to take the different noise levels of the recordings into account. In order to exclude the possibility that the results of the experiment are influenced by the threshold, we ran the same analysis with an absolute threshold in addition to the main analysis with a relative threshold. The results of this analysis can be found in the supplementary material.

Graph theory measures

Graph theory measures were derived from the thresholded connectivity matrices. Mean node degree, mean clustering coefficient, mean characteristic path length and maximum betweenness-centrality were calculated for each recording using algorithms implemented in the Brain Connectivity Toolbox (Rubinov and Sporns, 2010).[4]

Statistical analysis

An analysis of covariance (ANCOVA) with the graph theory measures as the dependent variables, age as a covariate and frequency band as a fixed factor was used. Age was treated as a continuous variable with precision to the day of testing. Frequency band was treated as a nominal variable with the frequency bands: 1–12 Hz, 12–25 Hz, and 25–40 Hz. All statistical analyses were carried out with SPSS 20.0 software (IBM Corp., NY) under Mac OS 10.7.4 (Apple Inc., CA).

[1] http://jerlab.psych.sc.edu/NeurodevelopmentalMRIDatabase/.

[2] http://surfer.nmr.mgh.harvard.edu.

[3] http://neuroimage.usc.edu/brainstorm/.

[4] https://sites.google.com/site/bctnet/.

Analysis of network structure

We applied eigenvalue decomposition to the average connection matrices of all participants for each frequency band to extract the modular structure of the networks (Clayden et al., 2013) (Fig. 3). The positive part of un-thresholded correlation matrices was used for principal network analysis (Fig. 3). The edge weight of the subnetworks identified in the average for all participants was calculated for each participant to characterise the relationship of connection strength within the network with age (Fig. 4).

Results

Correlation between graph theory measures and age

No significant effect of gender could be found in any of the outcome measures. Gender is therefore not included for any further analyses. There was a significant effect of age on mean node degree, mean clustering coefficient, characteristic path length and maximum betweenness-centrality (mean node degree: $F(1,92) = 7.62$, $p = 0.007$; mean clustering coefficient: $F(1,92) = 9.61$, $p = 0.003$;

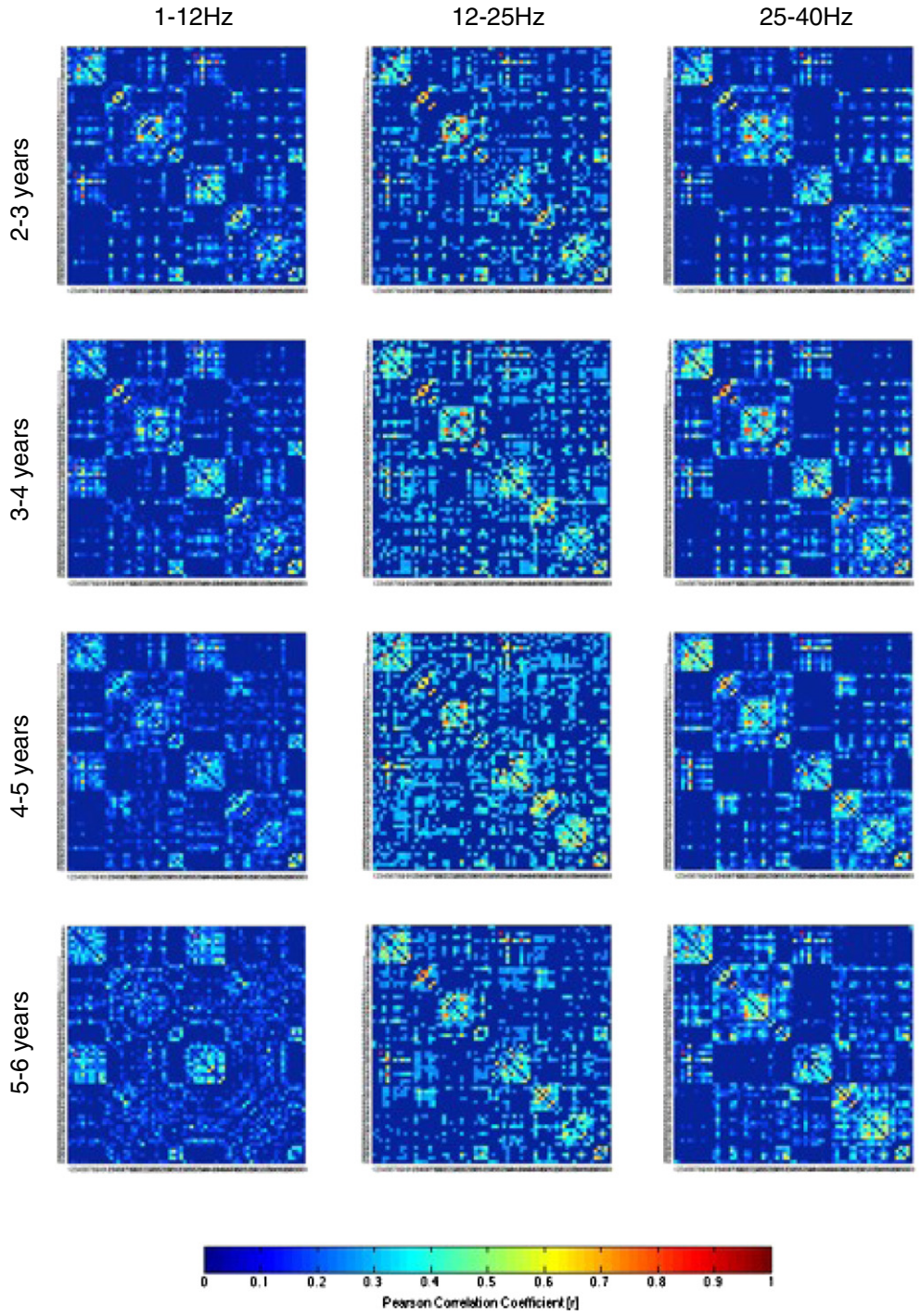

Fig. 1. Average connection matrices in age groups between 2 and 5 years in frequency bands from 1–12 Hz, 12–25 Hz and 25–40 Hz. Each column represents results for one frequency band: 1–12 Hz, 12–25 Hz, and 25–40 Hz. Each row represents one age group in the order: 2 years, 3 years, 4 years, and 5 years from top to bottom. The connectivity matrix shows the Pearson correlation efficient between any two nodes of the network. The nodes are numbered according to Table 1 for better overview.

Table 1
Overview of graph characteristics in different age groups for the frequency band from 1 to 12 Hz.

Age group	2 years	3 years	4 years	5 years
Number of participants	n = 8	n = 7	n = 10	n = 5
Gender	3 female	2 female	7 female	2 female
Number of connected vertices	68	68	68	68
Number of edges	3135	3198	3238	3278
Connection density	67.8%	69.2%	70.1%	70.98%
Mean edge weight	0.20	0.19	0.17	0.17
Mean node degree	24.21	26.1	27.23	28.41
Mean clustering coefficient	0.12	0.11	0.11	0.10
Mean shortest path length	0.07	0.07	0.06	0.07
Overview of graph characteristics in different age groups for the frequency band from 12 to 25 Hz				
Number of participants	n = 8	n = 7	n = 10	n = 5
Gender	3 female	2 female	7 female	2 female
Number of connected vertices	68	68	68	68
Number of edges	2963	3060	2980	3142
Connection density	64.1%	66.12%	64.45%	67.95%
Mean edge weight	0.31	0.33	0.31	0.33
Mean node degree	19.14	22	19.65	24.41
Mean clustering coefficient	0.16	0.17	0.16	0.16
Mean shortest path length	0.09	0.11	0.09	0.12
Overview of graph characteristics in different age groups for the frequency band from 25 to 40 Hz				
Number of participants	n = 8	n = 7	n = 10	n = 5
Gender	3 female	2 female	7 female	2 female
Number of connected vertices	68	68	68	68
Number of edges	3198	3060	2980	3142
Connection density	69.16%	66.18%	64.45%	67.94%
Mean edge weight	0.22	0.33	0.31	0.33
Mean node degree	26.06	22	19.65	24.41
Mean clustering coefficient	0.14	0.17	0.16	0.16
Mean shortest path length	0.08	0.11	0.09	0.12

Table 2
Cortical areas and their indices in the correlation matrices.
Cortical parcellation according to the Desikan–Killiany atlas performed under FreeSurfer v5.1.0.

Region	Index (left)	Index (right)
Caudal anterior cingulate	1	35
Caudal middle frontal gyrus	2	36
Frontal pole	3	37
Lateral orbitofrontal gyrus	4	38
Medial orbitofrontal gyrus	5	39
Pars opercularis	6	40
Pars orbitalis	7	41
Pars triangularis	8	42
Rostral anterior cingulate	9	43
Rostral middle frontal gyrus	10	44
Superior frontal gyrus	11	45
Inferior parietal gyrus	12	46
Isthmus cingulate	13	47
Paracentral gyrus	14	48
Postcentral gyrus	15	49
Precentral gyrus	16	50
Precuneus	17	51
Superior parietal gyrus	18	52
Supramarginal gyrus	19	53
Banks of the superior temporal sulcus	20	54
Entorhinal cortex	21	55
Fusiform gyrus	22	56
Inferior temporal gyrus	23	57
Insula	24	58
Middle temporal gyrus	25	59
Parahippocampal gyrus	26	60
Superior temporal gyrus	27	61
Temporal pole	28	62
Transverse temporal gyrus	29	63
Cuneus	30	64
Lateral occipital gyrus	31	65
Lingual gyrus	32	66
Pericalcarine cortex	33	67
Posterior cingulate cortex	34	68

characteristic path length: $F(1,92) = 4.82$, $p = 0.031$; maximum betweenness-centrality: $F(1,92) = 4.82$, $p = 0.031$). There was a significant influence of frequency band on characteristic path length and mean clustering coefficient (characteristic path length: $F(2,92) = 10.19$, $p < 0.001$; mean clustering coefficient: $F(2,92) = 9.43$, $p < 0.001$). Post-hoc contrasts show significant differences between frequency bands 1 and 2 (1–12 Hz & 12–25 Hz) as well as significant differences between the lowest and highest frequency bands in mean clustering coefficient (all p-values corrected for multiple comparison using Bonferroni correction: 1–12 Hz & 12–25 Hz: $p = 0.006$; 1–12 Hz and 25–40 Hz: $p < 0.001$). There were no significant differences in mean clustering coefficient between the frequency bands 2 and 3 (12–25 and 25–40 Hz: $p = 0.72$) (Fig. 2). The same pattern of differences was found for characteristic path length: significant differences between frequency bands 1 and 2 as well as 1 and 3 were found, but there was no significant difference between frequency bands 2 and 3 (all p-values corrected for multiple comparison using Bonferroni correction: 12–25 Hz and 25–40 Hz: $p = 0.003$; 1–12 Hz and 25–40 Hz: $p < 0.001$; 12–25 Hz and 25–40 Hz: $p = 0.74$).

In order to exclude the possibility that the observed associations between participant age and graph theory measures are due to the use of different head models for different age groups, the topography of the EEG was scrambled and subsequently processed as described. No correlations between participant age and graph theory measures were found for the scrambled data. The results of this analysis can be found in the Supplementary material.

Further, the goodness of fit between the predictions of the model and the original data was calculated for each recording. There was no significant effect of average goodness of fit (measured as R^2) on participant age ($p = F(1,92) = 0.161$, $p = .69$). There was also no significant difference in R^2 between frequency bands ($F(3,92) = 0.151$, $p = .93$). All values of R^2 were above 0.9 indicating a good fit between original data and the model (please refer to the Supplementary material for the details of the analysis).

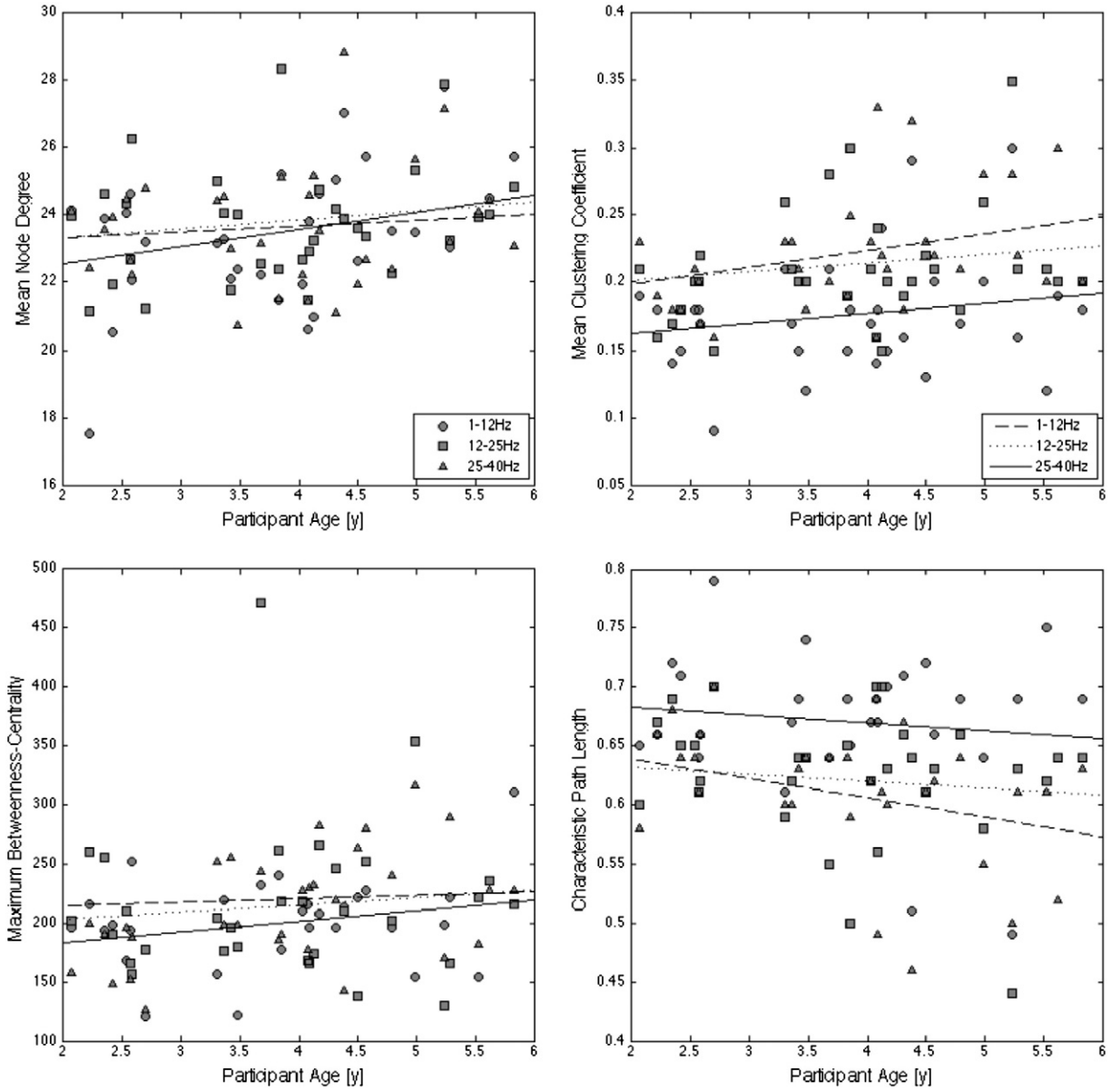

Fig. 2. Correlations between age and graph theory measures. Analysis of co-variance (ANCOVA) shows a main effect of age and frequency band (age: $F(5,85) = 3.465$, $p < 0.01$; Frequency band: $F(10,172) = 2.496$, $p < 0.01$). There was a significant effect of age on all graph measures ($F1(1,30) = 7.63$, $p < 0.01$; $F2(1,30) = 9.64$, $p < 0.01$; $F3(1,30) = 6.6$, $p < 0.05$; $F4(1,30) = 4.84$, $p < 0.05$). Frequency band had a significant effect on clustering coefficient and characteristic path length ($F_1(2,30) = 9.43$, $p < 0.001$; $F_2(2,30) = 10.91$, $p < 0.001$). The lines show least-square fitted lines for each frequency band to make linear associations easier to visually assess.

Development of network structure

An ANOVA of summed weight of interhemispheric connections with age as a covariate and frequency band as a fixed factor showed a significant effect of age and frequency band ($F(1,92) = 7.56$, $p = 0.007$; $F(2,92) = 5.92$, $p = 0.004$). Post-hoc comparison showed a significant difference between interhemispheric weight in the network for the lowest frequency band and the other bands (1–2: $p = 0.006$, 1–3: $p = 0.024$; 2–3: $p = 0.95$) (Fig. 4).

Next, we applied eigenvalue decomposition to the averaged correlation matrices of all ages for each frequency band to obtain relevant modules. The nodes that are part of the five principal networks were identified (Fig. 4.1). One network comprised mainly of left posterior areas (left superior temporal gyrus, left temporal pole, left transverse temporal gyrus, left lateral occipital gyrus and right posterior cingulate cortex). A second network contained the central areas on the right side (post-central gyrus, precuneus, supramarginal gyrus). A third network contained connections between anterior and posterior regions on the right side (caudal anterior cingulate, caudal middle frontal, precuneus, superior parietal gyrus, right middle temporal, cuneus, lateral occipital gyrus and lingual gyrus). Another large network contained mostly left frontal and central areas (caudal middle frontal gyrus, medial orbitofrontal gyrus, inferior parietal gyrus, paracentral gyrus, precuneus, superior parietal gyrus & right rostral anterior cingulate, paracentral gyrus). These networks are stable between the age groups under investigation. Correlations corrected for multiple comparison show no significant linear dependencies between age and summed edge weight within the subnetworks (two-tailed bivariate correlations, $abs(r) < 0.1$, $p > 0.01$ (Bonferroni corrected)).

In the frequency band from 12 to 25 Hz, principal network analysis also identified 5 modules (Fig. 4.2). One network contained temporal and occipital areas of the right hemisphere (middle temporal gyrus, lateral occipital gyrus among others). A second network consisted of posterior areas of the left hemisphere with connections to right central areas (left superior temporal gyrus, temporal pole, cuneus & right caudal middle frontal gyrus, precuneus, paracentral gyrus). A third

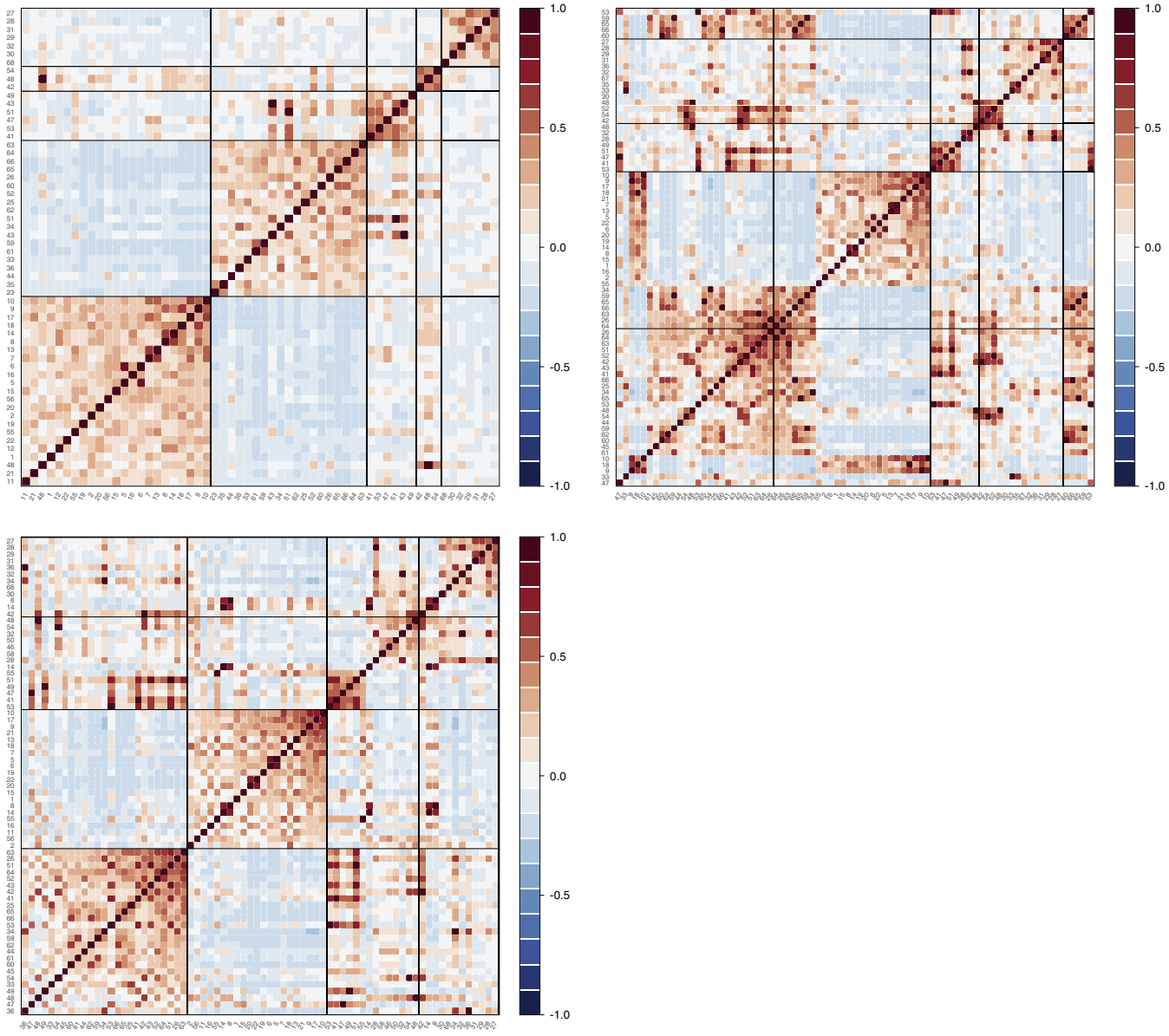

Fig. 3. Principal networks for the average network for all age groups for three frequency bands. Top left: 1–12 Hz; top right: 12–25 Hz; bottom left: 25–40 Hz. In each case, different subnetworks are delimited by unbroken black lines, and regions are ordered by their influence within each subnetwork.

network held connections between left frontal and right posterior areas (left rostral middle frontal gyrus, rostral anterior cingulate, precuneus & right lateral occipital cortex, transverse temporal gyrus). The fifth network contained connections within the right hemisphere. There was no correlation between summed edge weight within the principal networks and age (bivariate two-tailed correlations, $abs(r) < 0.1$, $p > 0.01$ (Bonferroni corrected)).

Similar to the other frequency bands, 4 modules were identified within the 25–40 Hz frequency band (Fig. 4.3). One network contained connections between central and posterior areas of the left hemisphere (left pars triangularis, paracentral gyrus, cuneus, posterior cingulate cortex). A second network consisted of connections between central and posterior areas of the right hemisphere (right paracentral gyrus, precentral gyrus, pars orbitalis, inferior parietal gyrus). The third subnetwork held left frontal and central areas (left caudal middle frontal gyrus, anterior cingulate, pars orbitalis, superior parietal gyrus, supramarginal gyrus). The fourth network contained connections within the right hemisphere. No significant correlations between summed edge weight within the principal networks and age were found (bivariate two-tailed correlations, $abs(r) < 0.1$, $p > 0.01$ (Bonferroni corrected)).

Discussion

The aim of this study was to apply connectivity analysis to source space regions of task-free EEG recordings of children between 2 and 6 years. In order to calculate the time series of cortical regions of interest, source activity was estimated through the use of age-appropriate head models based on averaged MRI scans. We demonstrated with this study that it is possible to estimate important network parameters from high-density EEG recordings. Key graph measures such as mean node degree, mean clustering coefficient and maximum betweenness-centrality changed with age. The increase in node degree together with the decline in path length and increase in maximum betweenness-centrality indicates that there is increased integration within functional modules of the network over development. The increase in clustering

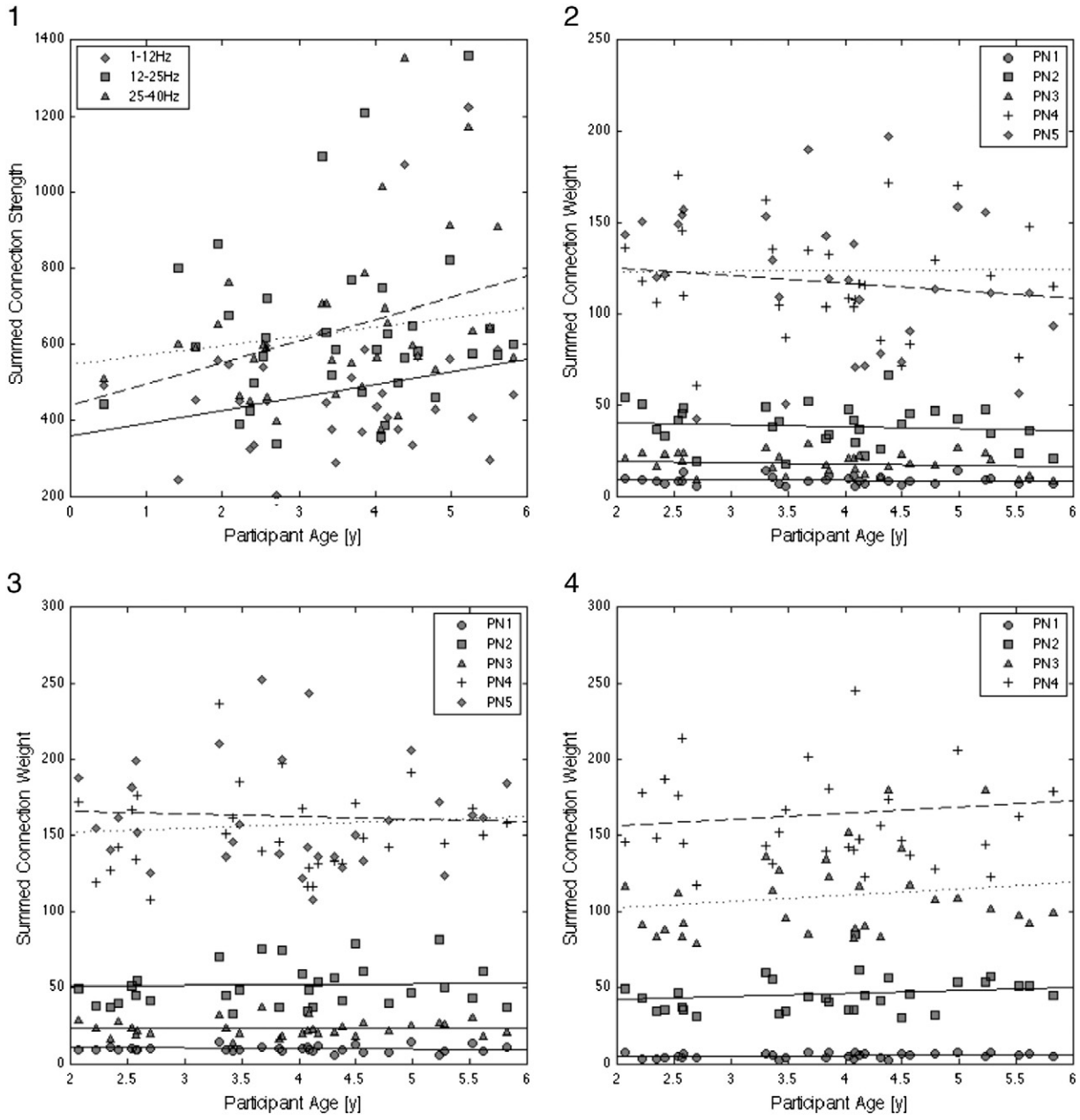

Fig. 4. Correlation between age and summed edge weight of key regions. There were no significant correlations between age and interhemispheric connection strength for all frequency bands. There was also no significant correlation between age and edge weight within the subnetworks identified with principal network analysis (see Fig. 3 for the principal networks). The lines show least-square fitted lines for each frequency band to make linear associations easier to visually assess.

coefficient suggests that associated nodes are more closely connected in the older children (Bullmore and Sporns, 2012; Fair et al., 2008; Power et al., 2010). A similar network organisation has previously been described in other imaging modalities such as cortical thickness analysis (He et al., 2007), diffusion tensor imaging (Hagmann et al., 2008; Honey et al., 2009) and resting-state functional MRI (Fair et al., 2008).

The correlation matrices show subnetworks of interconnected regions that are identifiable in all age groups and frequency bands. We demonstrated that these networks could be extracted through eigenvalue decomposition of the average networks. Correlations of edge weight and age indicated that connections within these subnetworks remain unchanged between 2 and 5 years of age. However, trends in correlation between age and the edge weight of interhemispheric connections suggested that interhemispheric connections increase between 2 and 5 years. The finding that edge weight within the functional subnetworks remained stable over age differs from the findings reported in the fMRI literature. Resting-state fMRI networks of children and adults show a general increase in connection strength (Fair et al., 2008, 2009; Power et al., 2010). Fair et al. report the largest increases for anterior–posterior connections. However, these studies compared children and adults (Fair et al., 2008). It is possible that the largest increases happen later in development. Based on reports of structural changes, adolescence is likely to be the period when the largest changes in the functional architecture are to be found (Hagmann et al., 2010). Given the low-cost and easy application of high-density EEG recordings, it will be possible to collect data from a larger sample of participants from early childhood to late adolescence. Acquiring longitudinal data will shed light on individual trajectories and link network architecture to various behavioural measures.

From an anatomical perspective, the subnetworks identified from the correlations of reconstructed EEG sources closely resemble the frontal and occipital hubs described in the fMRI literature (Power et al., 2010) and are consistent with the main network hubs of the DMN (Fox and Raichle, 2007; Fox et al., 2005). However, it is important to note that the spatial resolution of EEG source reconstruction is limited. Boundary element models together with minimum norm estimates allow to localise EEG source with a precision of up to 1 cm^2 for cortical sources (Babiloni et al., 2005; Schoffelen and Gross, 2009). Further, average MRI templates were used in this study. Source reconstruction might provide wrong results if the gyral and sulcal structure is very different from the average norm. Templates based on individual MR scans will minimise this error. Nevertheless, the results of the study demonstrate that important insights about the network organisation of the brain can be gained from source reconstruction based on average templates. This is an important result as individual MRI scans are not often available when studying children of ages 2–6.

EEG also allows researchers to take phase relationships and tem poral dynamics into account, which might open new windows to bridge fMRI network analysis and neural oscillations theory. The current study investigated the development of functional networks in three frequency bands. In general, the development of network structure and the hub regions within the networks of each frequency band are very similar. Still, differences were found in characteristic path length and clustering coefficient. Oscillations in different frequency bands are often linked to different physiological mechanisms. Frequencies below 12 Hz are associated with variation in large-scale excitability changes probably through neuromodulation (Laufs et al., 2003; Miller, 2007). Higher frequency oscillations were reported to correspond to local field potentials (Buzsàki et al., 2012; Whittingstall and Logothetis, 2009). Future studies will investigate the development of networks with different imaging modalities that are sensitive to different physiological changes. Computer models will help to understand how changes on various levels give rise to large scale changes in network architecture.

Acknowledgments

We want to thank Prof. John Richards, University of South Carolina, for granting us access to the Developmental MRI database and helpful discussions at the beginning of this work.

Conflict of interest

The authors have no conflict of interest to declare.

Appendix A. Supplementary data

Supplementary data to this article can be found online at http://dx.doi.org/10.1016/j.neuroimage.2013.06.003.

References

Babiloni, F., Cincotti, F., Babiloni, C., Carducci, F., Mattia, D., Astolfi, L., Basilisco, A., Rossini, P., 2005. Estimation of the cortical functional connectivity with the multimodal integration of high-resolution EEG and fMRI data by directed transfer function. NeuroImage 24, 118–131.

Barry, R.J., Clarke, A.R., McCarthy, R., Selikowitz, M., Johnstone, S.J., Rushby, J.A., 2004. Age and gender effects in EEG coherence: I. Developmental trends in normal children. Clin. Neurophysiol. 115, 2252–2258.

Bullmore, E., Sporns, O., 2009. Complex brain networks: graph theoretical analysis of structural and functional systems. Nat. Rev. Neurosci. 10, 186–198.

Bullmore, E., Sporns, O., 2012. The economy of brain network organization. Nat. Rev. Neurosci. 13, 336–349.

Buzsàki, G.G., Anastassiou, C.A., Koch, C., 2012. The origin of extracellular fields and currents — EEG, ECoG, LFP and spikes. Nat. Rev. Neurosci. 13, 407–420.

Cherkassky, V.L., Kana, R.K., Keller, T.A., Just, M.A., 2006. Functional connectivity in a baseline resting-state network in autism. Neuroreport 17, 1687.

Chu-Shore, C.J., Kramer, M.A., Bianchi, M.T., Caviness, V.S., Cash, S.S., 2011. Network analysis: applications for the developing brain. J. Child Neurol. 26, 488–500.

Clayden, J., Dayan, M., Clark, C.A., 2013. Principal networks. PLoS ONE 8 (4): e60997. http://dx.doi.org/10.1371/journal.pone.0060997.

Dale, A.M., Fischl, B., Sereno, M.I., 1999. Cortical surface-based analysis* 1: I. Segmentation and surface reconstruction. NeuroImage 9, 179–194.

Darvas, F., Pantazis, D., Kucukaltun-Yildirim, E., Leahy, R., 2004. Mapping human brain function with MEG and EEG: methods and validation. NeuroImage 23, 289.

De Vico Fallani, F., Astolfi, L., Cincotti, F., Mattia, D., Tocci, A., Marciani, M.G., Colosimo, A., Salinari, S., Gao, S., Cichocki, A., Babiloni, F., 2007. Extracting information from cortical connectivity patterns estimated from high resolution EEG recordings: a theoretical graph approach. Brain Topogr. 19, 125–136.

Dunn, L.M., Whetton, C., 1982. British Picture Vocabulary Scale. Nfer-Nelson Windsor.

Essex, M.J., Boyce, W.T., Goldstein, L.H., Armstrong, J.M., Kraemer, H.C., Kupfer, D.J., 2002. The confluence of mental, physical, social, and academic difficulties in middle childhood. II: Developing the MacArthur Health and Behavior Questionnaire. J. Am. Acad. Child Adolesc. Psychiatry 41, 588–603.

Evans, A.C., 2006. The NIH MRI study of normal brain development. NeuroImage 30, 184–202.

Fair, D.A., Cohen, A.L., Dosenbach, N.U.F., Church, J.A., Miezin, F.M., Barch, D.M., Raichle, M.E., Petersen, S.E., Schlaggar, B.L., 2008. The maturing architecture of the brain's default network. Proc. Natl. Acad. Sci. 105, 4028.

Fair, D.A., Cohen, A.L., Power, J.D., Dosenbach, N.U.F., Church, J.A., Miezin, F.M., Schlaggar, B.L., Petersen, S.E., 2009. Functional brain networks develop from a "local to distributed" organization. PLoS Comput. Biol. 5, e1000381.

Fischl, B., Sereno, M.I., Dale, A.M., 1999. Cortical surface-based analysis* 1: II: Inflation, flattening, and a surface-based coordinate system. NeuroImage 9, 195–207.

Fischl, B., Van Der Kouwe, A., Destrieux, C., Halgren, E., S√©gonne, F., Salat, D.H., Busa, E., Seidman, L.J., Goldstein, J., Kennedy, D., 2004. Automatically parcellating the human cerebral cortex. Cerebral Cortex 14, 11–22.

Fox, M.D., Raichle, M.E., 2007. Spontaneous fluctuations in brain activity observed with functional magnetic resonance imaging. Nat. Rev. Neurosci. 8, 700–711.

Fox, M.D., Snyder, A.Z., Vincent, J.L., Corbetta, M., Van Essen, D.C., Raichle, M.E., 2005. The human brain is intrinsically organized into dynamic, anticorrelated functional networks. Proc. Natl. Acad. Sci. U. S. A. 102, 9673.

Hagmann, P., Cammoun, L., Gigandet, X., Meuli, R., Honey, C.J., Wedeen, V.J., Sporns, O., 2008. Mapping the structural core of human cerebral cortex. PLoS Biol. 6, e159.

Hagmann, P., Deutsch, D., Sporns, O., HenthornN, T., Madan, N., Dolson, M., et al., 2010. White matter maturation reshapes structural connectivity in the late developing human brain. Proceedings of the National Academy of Sciences. http://dx.doi.org/10.1073/pnas.1009073107.

Hämäläinen, M.S., Ilmoniemi, R., 1994. Interpreting magnetic fields of the brain: minimum norm estimates. Med. Biol. Eng. Comput. 32, 35–42.

He, B., Wang, Y., Wu, D., 1999. Estimating cortical potentials from scalp EEGs in a realistically shaped inhomogeneous head model by means of the boundary element method. IEEE Trans. Biomed. Eng. 46, 1264–1268.

He, B., Yang, L., Wilke, C., Yuan, H., 2011. Electrophysiological imaging of brain activity and connectivity — challenges and opportunities. IEEE Trans. Biomed. Eng. 58, 1918–1931.

He, Y., Chen, Z.J., Evans, A.C., 2007. Small-world anatomical networks in the human brain revealed by cortical thickness from MRI. Cereb. Cortex 17, 2407–2419.

Hipp, J.F., Hawellek, D.J., Corbetta, M., Siegel, M., Engel, A.K., 2012. Large-scale cortical correlation structure of spontaneous oscillatory activity. Nat. Neurosci. 15, 884–890.

Homae, F., Watanabe, H., Otobe, T., Nakano, T., Go, T., Konishi, Y., Taga, G., 2010. Development of global cortical networks in early infancy. J. Neurosci. 30, 4877–4882.

Honey, C.J., Sporns, O., Cammoun, L., Gigandet, X., Thiran, J.P., Meuli, R., Hagmann, P., 2009. Predicting human resting-state functional connectivity from structural connectivity. Proc. Natl. Acad. Sci. U. S. A. 106, 2035–2040.

Laufs, H., Kleinschmidt, A., Beyerle, A., Eger, E., Salek-Haddadi, A., Preibisch, C., Krakow, K., 2003. EEG-correlated fMRI of human alpha activity. NeuroImage 19, 1463–1476.

Logothetis, N.K., 2008. What we can do and what we cannot do with fMRI. Nature 453, 869–878.

Marshall, P.J., Bar-Haim, Y., Fox, N.A., 2002. Development of the EEG from 5 months to 4 years of age. Clin. Neurophysiol. 113, 1199–1208.

Menon, V., 2011. Large-scale brain networks and psychopathology: a unifying triple network model. Trends Cogn. Sci. 15, 483–506.

Michel, C.M., Murray, M.M., 2011. Towards the utilization of EEG as a brain imaging tool. NeuroImage 61, 371–385.

Miller, R., 2007. Theory of the normal waking EEG: from single neurones to waveforms in the alpha, beta and gamma frequency ranges. Int. J. Psychophysiol. 64, 18–23.

Murias, M., Swanson, J.M., Srinivasan, R., 2007. Functional connectivity of frontal cortex in healthy and ADHD children reflected in EEG coherence. Cereb. Cortex (New York, N.Y. 1991) 17, 1788–1799.

O'Reilly, H., 2012. Epilepsy in Infancy: Cognitive & Social Developmental Outcome at 3–5 years. University College London, UK.

Palmer, H., 2010. Optogenetic fMRI sheds light on the neural basis of the BOLD signal. J. Neurophysiol. 104, 1838.

Power, J.D., Fair, D.a, Schlaggar, B.L., Petersen, S.E., 2010. The Development of Human Functional Brain Networks. Neuron 67, 735–748.

Rubinov, M., Sporns, O., 2010. Complex network measures of brain connectivity: uses and interpretations. NeuroImage 52, 1059–1069.

Sanchez, C.E., Richards, J.E., Almli, C.R., 2012. Neurodevelopmental MRI brain templates for children from 2 weeks to 4 years of age. Dev. Psychobiol. 54, 77–91.

Schoffelen, J.M., Gross, J., 2009. Source connectivity analysis with MEG and EEG. Hum. Brain Mapp. 30, 1857–1865.
Shulman, G.L., Fiez, J.A., Corbetta, M., Buckner, R.L., Miezin, F.M., Raichle, M.E., Petersen, S.E., 1997. Common blood flow changes across visual tasks: II. Decreases in cerebral cortex. J. Cogn. Neurosci. 9, 648–663.
Sporns, O., 2002. Graph theory methods for the analysis of neural connectivity patterns. Neuroscience databases. A practical guide, pp. 169–183.
Stroganova, T.A., Orekhova, E.V., 2007. EEG and infant states. In: de Haan, M. (Ed.), Infant EEG and Event-Related Potentials. Psychology Press, Hove.
Sylvain, B., John, C., Dimitrios, P., Richard, M., 2011. Brainstorm: a user-friendly application for MEG/EEG analysis. Comput. Intell. Neurosci. 2011, 1–13.
Thatcher, R.W., North, D.M., Biver, C.J., 2008. Development of cortical connections as measured by EEG coherence and phase delays. Hum. Brain Mapp. 29, 1400–1415.
Uhlhaas, P.J., Roux, F., Rodriguez, E., Rotarska-Jagiela, A., Singer, W., 2010. Neural synchrony and the development of cortical networks. Trends Cogn. Sci. 14, 72–80.
Uhlhaas, P.J., Roux, F., Singer, W., Haenschel, C., Sireteanu, R., Rodriguez, E., 2009. The development of neural synchrony reflects late maturation and restructuring of functional networks in humans. Proc. Natl. Acad. Sci. U. S. A. 106, 9866–9871.
Van den Heuvel, M., Stam, C., Boersma, M., Hulshoff, P.H., 2008. Small-world and scale-free organization of voxel-based resting-state functional connectivity in the human brain. NeuroImage 43, 528–539.
Watts, D.J., Strogatz, S.H., 1998. Collective dynamics of small-world networks. Nature 393, 440–442.
Whittingstall, K., Logothetis, N.K., 2009. Frequency-band coupling in surface EEG reflects spiking activity in monkey visual cortex. Neuron 64, 281–289.
Yu, S., Huang, D., Singer, W., Nikolic, D., 2008. A small world of neuronal synchrony. Cereb. Cortex 18, 2891–2901.